Check for updates

Understanding doping strategies in the design of organic electrode materials for Li and Na ion batteries: an electronic structure perspective†

Johann Lüder, [ID] Mun Ho Cheow and Sergei Manzhos [ID] *

In this paper, we present a systematic study of the effects of p- and n-doping in small molecules on the voltage and capacity of organic electrode materials for electrochemical batteries. In particular, coronene, phenalene derivatives as well as disodium terephthalate and related fused ring derivatives, representing often used building blocks in organic electrode materials, are chosen as model systems. We show that p-doping can drastically increase the binding strength to Li or Na and is therefore an effective strategy to design organic electrode materials for both lithium and sodium ion batteries. It could also be used to increase the theoretical capacity. On the other hand, n-doping generally has a much smaller effect on the voltage. The effects of n- and p-doping are rationalized based on the analysis of changes they induce in the band structure as well as in the molecular structure.

Introduction

Batteries have revolutionised the way electronic devices are used today and consequently many aspects of human life and society, too. Today, information can be obtained on the go with a variety of mobile devices. Other applications can be found in clinical use, for example, to monitor key health figures as well as life securing devices like artificial cardiac pacemakers, which are routinely used.[1] Most high-performance batteries depend on lithium (Li) as the cation in the redox reaction.[2–4] Lithium-ion batteries offer high energy densities and stable cycling rates, which led to their widespread commercialization.[5] Examples of their applications range from portable electronic devices,[6] grid-level electric energy storage of renewable energies[7–9] to electric mobility.[10,11] High performance storage systems based on rechargeable metal-ion batteries[12–14] can be used for electro-mobility and grid storage, but improvements are still needed in performance as well as in sustainability and scalability over the available Li ion batteries.

Lithium-ion batteries are often made of materials containing elements like cobalt, which are expensive and/or constitute a potential environmental threat.[15,16] On the other hand, lithium is required, which makes this element a valuable resource. Lithium is relatively scarce and geographically concentrated. Abundant elements like sodium (Na) are in general an alternative to lithium. However, due to a higher Na/Na⁺ potential

than that of Li/Li⁺, sodium ion batteries have often lower voltages. Because of the larger ionic radius of Na⁺ they also generally have a worse rate performance due to the slow kinetics of Na in commonly used (inorganic) active materials. Nonetheless, potential applications have triggered many post-lithium battery investigations[3,17–19,20] with promising outlooks.

An alternative to inorganic batteries is organic batteries,[21,22] which are constructed from molecules or polymers,[23–27] and are therefore a suitable choice for an environmentally friendly alternative to conventional batteries.[8] In general, electrode materials have a conducting part and a redox/active part. Well-known examples of organic molecules/polymers with a redox active part are carboxylates,[13,28] others have a radical character[29] or sulfuric groups.[30,31] Many different organic molecules and polymers have been identified over the last decades.[4,9,14] Moreover, the possibility of functionalization with, for example, cyano and other chemical groups drastically increases the number of possible electrode materials.[9] In particular, small organic molecules such as terephthalates and quinone derivatives have attracted attention as anode materials in organic batteries.[32,33] They offer large specific capacities due to their small size. In combination with cations from abundant elements, as mentioned above, such as sodium, potassium or magnesium, environmentally friendly and low-cost post-lithium organic batteries[18,20,34–36] can be constructed.

The development of practical organic batteries still faces multiple challenges including stability issues, low reversible capacities as well as voltages, which are either too low for cathodic operation or too high for anodic operation.[26,38] A detailed understanding of the charge–discharge mechanism

*Department of Mechanical Engineering, National University of Singapore,
21 Lower Kent Ridge Rd, Singapore 119077, Singapore. E-mail: mpemanzh@nus.edu.sg*

This journal is © the Owner Societies 2017

Phys. Chem. Chem. Phys., 2017, **19**, 13195–13209 | **13195**

is required to perform a rational design rather than an *ad hoc* approach to find new electrode materials for organic batteries.

The approach to design, however, must consider the chemistry of the electrode material. Organic electrodes can operate *via* oxidation or reduction.[24,39,40,41] The former is often used in organic cathode materials, whereby in the battery charged state, the cathode material is oxidized and coordinates to the anions of the electrolyte. During discharge, the active material is reduced back to neutral as Li ions released by the anode coordinate to the anions. In this mechanism, the oxidation potential, and therefore the energy of the highest occupied molecular orbital (HOMO), is the key determinant of the voltage. In the reduction mechanism, the active organic material is lithiated (or sodiated). The lithiation/sodiation causes the reduction of the active material by the valence electrons of Li/Na and consequently the reduction potential (and the energy of the lowest unoccupied molecular orbital (LUMO)) is a key determinant of the voltage. Structural changes induced by lithiation/sodiation also influence the voltage.[32] The two mechanisms can also be used in combination.[42,43] Multiple organic electrode materials, in particular, those based on small molecules, and operating by reduction have been proposed.[44–46] These typically exhibit voltages more suitable for anodic operations. There are few reports on use of molecular materials operating by reduction as cathodes. For example, TCNQ (tetracyanoquinodi-methane) has shown a plateau around 3 V.[47] Small organic molecules capable of coordinating multiple Li or Na atoms are especially appealing if high specific capacities are of importance. It would be advantageous to have small molecules also providing high voltages during lithiation/sodiation to obtain high energy density and power.

Depending on the application of a molecule, different design strategies can be used. Specifically, the doping approach can be used to improve voltages for both types of organic batteries through altering the energies of frontier orbitals. Both p- and n-doping have been reported in the experimental literature to improve various aspects of electrode performance including voltages and capacities.[5,48,49] Theoretical rationalization of putative effects of different types of doping is however often missing or counterintuitive claims or results have been reported. For example, the reports of increased voltages and/or specific capacities with n-doping go against the notion that such doping would result in fewer lower-energy states to be occupied by the valence electrons of Li/Na. On the other hand, works reporting increased voltage with p-doping go along with the notion that such doping creates lower-energy states.[44,50] Clearly, a systematic understanding of the effects of p- and n-doping on the voltage and capacity of organic electrode materials, which would relate these effects to the changes in electronic structure, is required. From a solid-state perspective, doping is well understood: the band structure can be modified by n-doping which reduces the host material or p-doping which oxidizes it. This determines the available states for the valence electrons of Li/Na and thereby modulates the Li/Na binding energy and therefore the voltage.

Many potential organic materials suitable for applications as active electrode materials have been identified. The earlier mentioned quinones and TCNQ are only two examples of small organic electrode building blocks; many more exist. Graphene-flakes (GFs), in general, could be another class of building blocks. For instance, coronene and phenalene are two molecules which represent GFs. In particular, coronene used as a cathode has high cyclic stability in dual-ion batteries.[39] Through the tunable size of GFs, their properties like the HOMO–LUMO (HL) gap as well as the position of their HOMO and LUMO in the valence spectrum can be modified. While this class of functional materials has no redox active groups, functionalization can be used to modify redox properties. While the benzene molecule might be regarded as the smallest GF, the terephthalate (TP) molecule might be considered as a benzene molecule functionalized with two carboxylic groups. The latter functional group is one of many, and other combinations are possible. The Na_2TP molecule, in particular, has attracted significant attention in the field of organic battery research already.[51–53] Especially the metal organic frameworks that it builds with Li, K, Na and Ag have been investigated from experimental and theoretical perspectives.[42,51,54,55] Furthermore, it is rather easy to modify organic molecules, and fused-ring structures can also be introduced into the Na_2TP molecule. For example, a two peri-fused benzene molecule is a GF; with the addition of two carboxylic groups, it becomes a fused-ring derivative of the Na_2TP molecule.[56,57] Therefore, fused ring and carboxylate based structures are good prototypical examples to study any effects of doping, and therefore they are used in this paper.

In this theoretical study, we show how the capacity of organic batteries and their voltage can be designed *via* direct substitutional doping. We therefore provide effective design paths for materials for organic lithium and sodium batteries. Substitutional doping of aromatic rings in molecules is used for this purpose. The systematically considered dopants are boron (B) and nitrogen (N) atoms that replace carbon (C) atoms; these act, respectively, as single p- and n-dopants. Moreover, as their size is comparable to that of carbon, such doping is expected to be feasible, and we can analyse the effects due to the modulation of the electronic structure (as opposed to effects due to large structural changes). In particular, we explain how n- and p-doping can be used to design organic materials with HOMO and LUMO levels suitable for use as anodes and cathodes. We first consider coronene and phenalene where the effect of doping of the aromatic ring structure is analysed. Then we consider disodium terephthalate (TP)[28,52] and its fused-ring derivatives. These systems have at least one aromatic ring and two redox active carboxyl groups. This highlights the inter-action between the doped ring structure and the redox active groups.

We show that p-doping can drastically increase the binding strength to Li or Na and is therefore an effective strategy to design organic anode materials for both lithium and sodium ion batteries. It could also be used to increase the theoretical capacity. On the other hand, n-doping generally has a much smaller effect on the voltage.

Computational details

Method

Density functional theory (DFT) calculations were carried out using the Gaussian09 package.[58] The many-body effects were

13196 | *Phys. Chem. Chem. Phys.,* 2017, **19**, 13195–13209

This journal is © the Owner Societies 2017

approximated with the B3LYP hybrid functional.[59–61] The electronic states were described by the 6-31+G(d,p) basis set.[62,63] It was tested for selective cases against the 6-31++G(d,p) and 6-311+G(d,p) basis sets to ensure convergence.

The formation energies defined here per lithium/sodium atom E_{fo} were computed as the total energy difference between the fully relaxed lithiated/sodiated system ($E_{mol+Li/Na}$) and the individual parts, i.e. the fully relaxed molecule (E_{mol}) and n times the energy of an isolated sodium or lithium atom ($E_{Li/Na}$):

$$E_{fo} = (E_{mol+Li/Na} - E_{mol} - nE_{Li/Na})/n \qquad (1)$$

The formation energy with respect to the cohesive energy ($E_{coh}^{Li/Na}$) of the charge carrier (ca. -1.67 eV for Li and -1.1 eV for Na)[64,65] corresponds here to the theoretical open-circuit voltage[66] according to

$$V = -(E_{fo} - E_{coh}^{Li/Na})/q \qquad (2)$$

where q is the charge of one electron. Eqn (2) results from approximating the reaction free energy by the internal energy, which is a valid simplification if entropy effects are negligible.[67] To obtain the global minimum structures, many initial geometries were used to compute the attachment energy of Li/Na atoms onto the molecule (see the ESI†). After attachment onto the molecule, the Li/Na atoms are effectively ionized. In total, more than 3000 structure optimizations were carried out for the five different molecules and their doped versions including their lithiation and sodiation. At least four Li/Na atoms were attached on each molecule to study their interaction. If the formation energy was larger than the cohesive energy of the respective metal, further atoms were added until the formation energy converges within ca. 0.1 eV per attached alkali atom. The binding energies are computed for molecules in the gas phase. Solvent or other environment effects such as the crystal structure can change the binding strength between molecules and Li/Na atoms. However, here we are not concerned with the effects which are specific to each end use, but effects on binding energies due to changes in the electronic structure caused by doping. While the magnitude of the binding strength will depend on the environment, it will not affect the conceptual conclusions about the effects of doping.

According to eqn (2), the voltages are estimated with respect to the cohesive energies, which are taken to represent the standard potential of the alkali metals. All voltages given in this study refer to those. If $V > 0$, the material can in principle operate as an active electrode material.

The strain energy contributions to the total binding energy between the molecule and alkali atom(s) were estimated from the difference in the total energy between the free molecule in its fully relaxed structure and the deformed molecule (without considering the alkali atoms). In the latter case, all additional alkali atoms are removed from the fully relaxed structures while the (frozen) molecule keeps its geometry.

The molecular systems in detail

As mentioned above, the first type of system is graphene flakes (GFs), shown in Fig. 1(a)–(c). We consider the coronene molecule (a),

the phenalene molecule (b) and the deprotonated phenalene (c), i.e. we consider fused ring systems of different sizes. Due to the simple structure of the GFs tested here, a solid understanding of the doping mechanisms is obtained.

There are two non-equivalent sites in the carbon backbone of phenalene where the dopants are bonded only to carbon atoms. This will not cause major structural changes like the
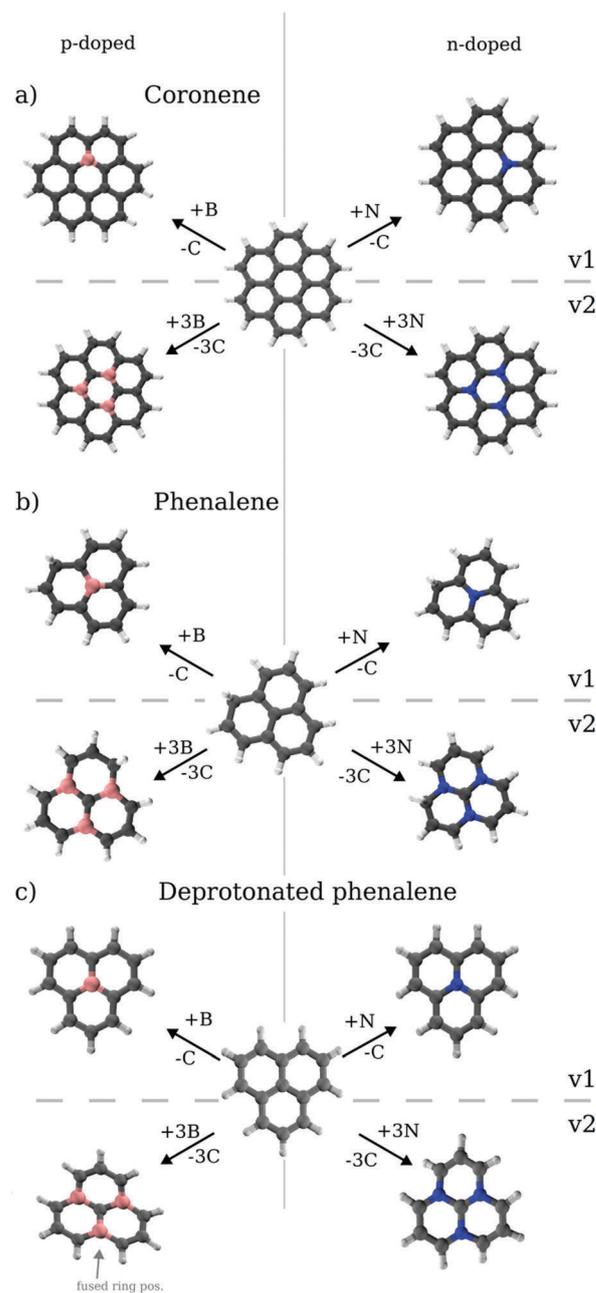

Fig. 1 Considered GF (graphene flake) structures (a) coronene, (b) phenalene and (c) deprotonated phenalene. The schematic shows for the boron-doped (left), pristine (middle) and nitrogen-doped (right) versions of the GFs. In case of doped structures, the upper ones have one dopant (v1), while the lower structures have three (v2), respectively. Here and elsewhere, carbon atoms are shown in grey, nitrogen atoms in blue, boron atoms in pink, and hydrogen atoms in white. The fused ring site of the dopant is indicated in (c). VMD[37] was used to plot the presented structures.

loss of an H atom. The two ways of doping studied here, with one and three doped sites, are shown in Fig. 1. In the first version (v1), the central C atom is replaced ($C_{12}XH_{10}$) (X = {B, N}) and in the 2nd version (v2), three outer fused-ring C atoms are changed ($C_{10}X_3H_{10}$). Doping sites for coronene are chosen similarly. Even though some of these structures may be challenging to synthesise, important theoretical insights can be obtained with them. We therefore consider different amounts of dopants and different molecular sizes. Moreover, we also include the phenalene molecule in its deprotonated form to facilitate comparison with the coronene; deprotonation can also be caused in practice by a chemical environment.

As mentioned above, we also consider molecules with active redox centers. Disodium terephthalate (Na_2TP) is a salt of terephthalic acid containing two Na atoms at the redox active carboxyl groups. Compared to the aromatic ring structure of GFs, the redox active groups represent an additional branch in organic battery design. Na_2TP is a promising anode material for Li and Na ion batteries.[28,52,53,68] Interestingly, its sodiation can occur on its aromatic ring after an initial reaction on the carboxyl groups.[28] We investigate if the doping in the aromatic ring structure can be applied to systems with redox active groups in the same way as for the GFs.

In this study, we focus on molecules with dicarboxylic groups in which the dopant is located in a quasi-fused ring or/and fused ring position, see Fig. 2 version 2 (v2) and Fig. 3 versions 1, 2 and 3. These sites have in common that the dopant atom is bonded to other carbons atoms only. At other sites in the benzene ring, it is not uncommon that a C–H group is replaced with a substituent. For example, a commonly known substitution reaction can yield pyridinedicarboxylic acid (NTP) which can also form a disodium salt, see Fig. 2 version 1 (v1). Because, as we will show later, the removal of a hydrogen atom during substitutional doping adds further modification to the electronic structures, the doping effects are studied here only for the Na_2TP molecule.

Doping of fused-ring (fr) naphthalate disodium salts based on the naphthalene dicarboxylic acid is also investigated.

disodium naphthalate

Fig. 3 Structures of the fused-ring disodium naphthalate salt. p- and n-doped versions of the fused ring naphthalate disodium salt are distinguished between version one (v1), two (v2) and three (v3).

The fused-ring structures allow for a more direct comparison to the GF cases as well as to obtain insights into the effects due to size. Fig. 3 shows the fused-ring naphthalate disodium salt and its doped variants. Three different versions were modelled here. In version one (v1), the dopant is between the peri-fused benzene rings. Version two (v2) is more similar to the Na_2TP's v2 with the dopant at the quasi-fused position connected to the carboxyl group. The third version (v3) includes both sites as shown in Fig. 3. These versions test the influence of the distance between redox active groups and the doped sites as well as of the concentration of dopants.

Results and discussion

In the following, we first present the effect of p- and n-doping on the electronic structure of individual molecules. We then analyse their effect on properties directly related to battery performance. Specifically, we study binding energies to different numbers of Li/Na and provide estimates of voltage–capacity curves.

Effect of doping on molecular properties

Graphene flakes. The optimised structures of the coronene molecule and its doped versions remain mostly flat. These structures can be seen in Fig. 1(a).

The electronic structures of these molecules can be understood by analysing the densities of states (DOS) of pristine and doped molecules with different numbers of n- and p-dopants,
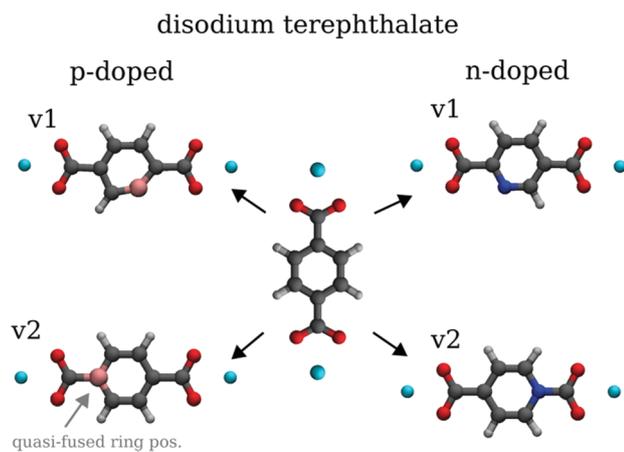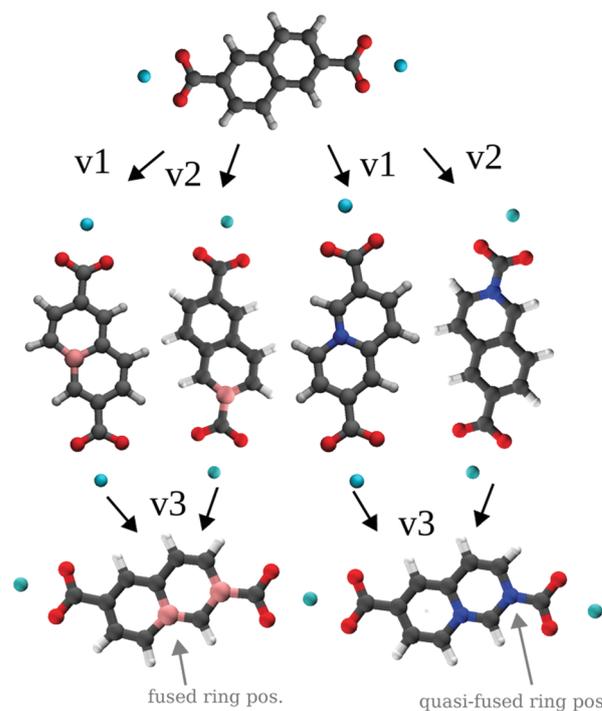

disodium terephthalate

Fig. 2 Structures of the disodium terephthalate salt (centre) and its boron (left) and nitrogen (right) doped versions. Here and elsewhere, alkali atoms are shown in cyan. The quasi-fused ring site is indicated in the p-doped structure v2.

13198 | *Phys. Chem. Chem. Phys.*, 2017, **19**, 13195–13209

This journal is © the Owner Societies 2017

shown in Fig. 4. Fig. 4 shows that substitutions with B and N atoms have an effect similar to p- and n-doping, respectively. With the B atom as the dopant, an unoccupied state – a hole – is created near the valence level of the molecule, while with the N atom, a filled state appears in the HOMO–LUMO gap. With 3 dopants, 3 such states are created. The creation of one hole state for single p-doping shifts the LUMO by more than 2 eV down. The new LUMO, as it becomes unoccupied, corresponds to the pristine molecule's HOMO as shown in Fig. 5. Specifically, Fig. 5 compares the nodal structures of the frontier orbitals, including LUMO+1 and HOMO−1, of the coronene molecule and its singly doped versions. Spin channels are separated in the left and right columns. While it is evident that the perturbation due to doping is large enough to cause orbital reordering, the main effects of reduction and oxidation, i.e. occupying and emptying of the frontier orbitals, is achieved. In particular, the new LUMO (spin down) of p-doped coronene has the same nodal structure as the HOMO (spin up) of coronene and the new HOMO (spin up) of n-doped coronene has a similar nodal structure as the LUMO of coronene. With more p-dopants, more empty states are created (not shown in Fig. 5); however, the larger perturbation causes the nodal structure of the orbitals to change to a larger extent. With more p-dopants, the HOMO energies shift to even lower energies as more and more empty states are created. On the other hand, one n-dopant introduces a filled state in the gap, which corresponds to the LUMO of the pristine molecule, creating a HOMO state shifted up (see Fig. 4 and 5). In other words, the LUMO of the pristine system becomes occupied and shifts

down in energy by about 1.5 eV. Also with more n-dopants, more occupied states are introduced, see Fig. 4, where the band structure of coronene and coronene doped with one or three p- or n-dopants is shown. Again, the larger perturbation due to more dopants causes larger changes in the nodal structure of the frontier orbitals. We note that the energies of all orbitals (i.e. other than those created by doping) also change due to many-body effects and changes in the molecular structure.

Table 1 compiles the changes in the HOMO and LUMO energy levels caused by p- and n-doping in coronene. It also provides the values of relative shifts of these energy levels with respect to the pristine coronene molecule. These relative changes are given in brackets. The HOMO–LUMO gap of the pristine coronene was computed to be 4.07 eV. In all doped versions of coronene, the gap drastically reduces to values between 1.06 and 1.54 eV. The gap decreases with an increase in dopant concentration and p-doping reduces the gap stronger than n-doping.

As described above, for applications in organic battery materials, the changes in the HOMO and LUMO positions are more important. p-Doping strongly affects the LUMO position. For coronene, shifts of ca. 2.8 eV were observed for triple p-doping whereas n-doping has similar effects on the HOMO positions with shifts seen here up to 2.6 eV. Of course, this influence is mainly a consequence of emptying and occupying states with additional electronic and structural relaxations. Structural effects are more noticeable at higher dopant concentrations, which cause larger changes in the overall electronic structure, too. However, it must be emphasized that these molecular structures are very similar to each other and only the chemical composition defines the major modifications. The changes in the electronic structure of coronene are thus very similar to those seen in doped solids. While substitutional doping for very small aromatic molecules like benzene is not practical or can lead to significant structural changes, the feasibility is higher for larger structures. Already the pentalene molecule (C_8H_6) is large enough to practically realize substitution of a C atom with a B atom.[69] This becomes even more evident with respect to larger graphene flakes. Graphene is the well-known limit of an infinite two-dimensional carbon flake.[70] Its doped forms with boron or nitrogen atoms are also well studied experimentally.[71–74] Thus, the understanding gained with the coronene molecule can be translated to other molecular systems.

In contrast, graphene flakes smaller than coronene may suffer structural destabilization when doped. The molecular structures of phenalene and deprotonated phenalene are more sensitive to doping, as shown in Fig. 1(b) and (c), respectively. The pristine molecules are planar in both cases. Triple doping can have substantial influence on the structure. The triple p-doped deprotonated phenalene is distorted as one benzene ring is tilted out of the molecular plane. The triple n-doped deprotonated phenalene is similarly distorted, and triple n-doped phenalene is buckled. In contrast, triple p-doped phenalene remains flat and both, single doped phenalene and deprotonated, are planar, too.

Similar changes in the electronic structure were observed for phenalene and deprotonated phenalene, as summarised in
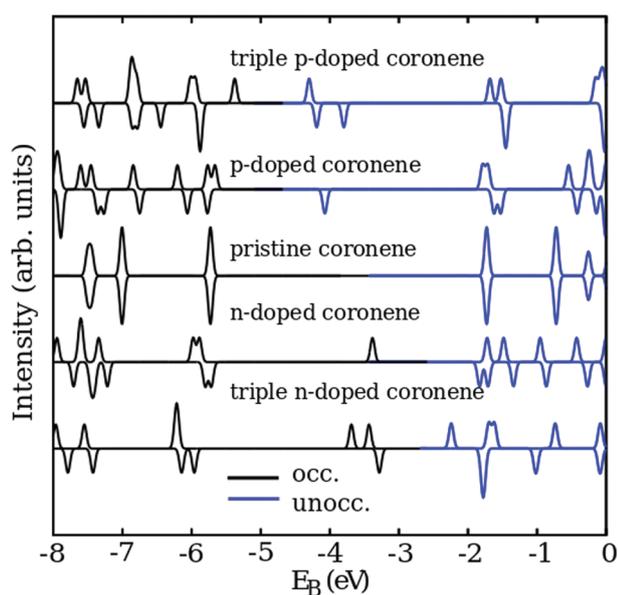

Fig. 4 Densities of states of coronene and coronene doped with one or three n- or p-dopants. The occupied (occ.) and the unoccupied (unocc.) states are shown in black and blue, respectively. Top to bottom: DOS of the triple p-doped (3p), single p-doped (p), pristine, single n-doped (n) and triple n-doped (3n) coronene. Spin channels are separated. All DOS displayed in this article were obtained by convoluting the eigenvalues of the electronic states with a Gaussian function with a FWHM (full width half maximum) of 0.175 eV.
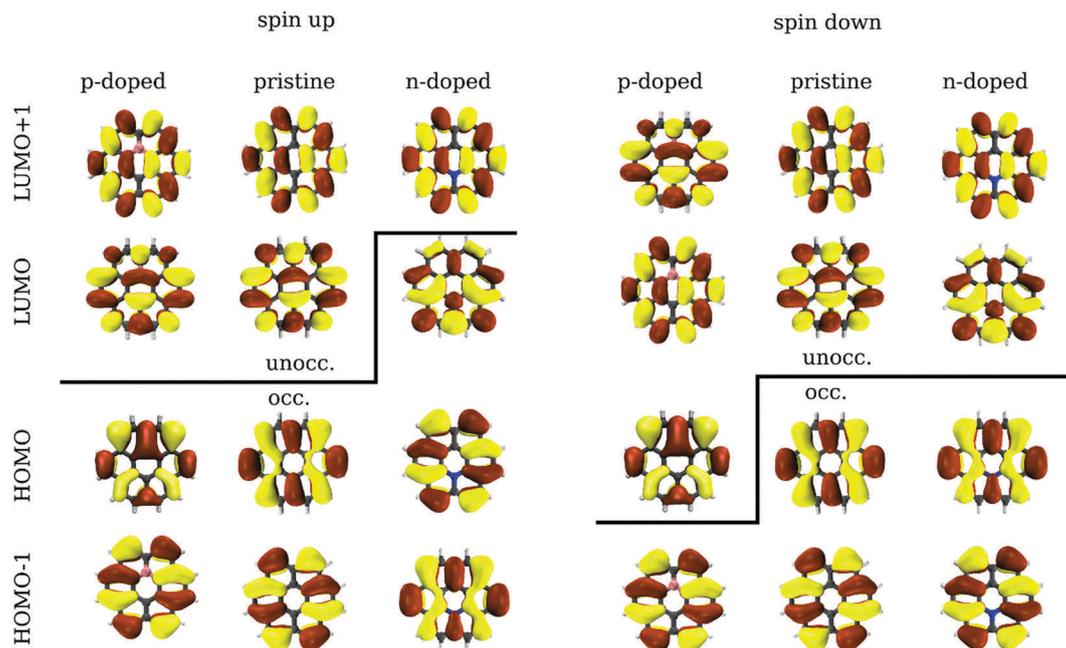
Fig. 5 Selected orbitals of the coronene and its doped versions. Different phases of the orbitals are shown as orange and yellow iso-density surfaces at values of $0.02\ e^{0.5}\ \text{Å}^{-3}$. Occupied and unoccupied orbitals are separated with a solid black line for the spin-up (left panel) and the spin-down (right panel) channel. The four selected orbitals around the frontier orbitals of the pristine molecule are ordered from bottom to top in order of increasing energy; they are HOMO−1, HOMO, LUMO and LUMO+1. Their counterparts in the p- and n-doped versions can be compared across rows to the orbitals of the pristine molecule.

Table 1 HOMO and LUMO eigenvalues of coronene and its doped versions. Values in brackets give the change relative to the pristine case

	HOMO (eV)	LUMO (eV)	Gap (eV)
p-Doped v2	−5.54	−4.48	1.06
	(0.21)	(−2.79)	(−3.01)
p-Doped v1	−5.69	−4.33	1.36
	(0.07)	(−2.65)	(−2.76)
Pristine	−5.76	−1.69	4.07
n-Doped v1	−3.29	−1.75	1.54
	(2.47)	(−0.06)	(−2.53)
n-Doped v2	−3.14	−1.83	1.31
	(2.61)	(−0.14)	(−2.76)

Table 2 HOMO and LUMO eigenvalues of phenalene and its doped versions. Values in brackets give the change relative to the pristine case

	HOMO (eV)	LUMO (eV)	Gap (eV)
p-Doped v2	−6.02	−4.23	1.78
	(−0.50)	(−2.71)	(−2.21)
p-Doped v1	−5.61	−3.94	1.68
	(−0.10)	(−2.42)	(−2.31)
Pristine	−5.51	−1.52	3.99
n-Doped v1	−3.31	−1.62	1.69
	(2.21)	(−0.09)	(−2.30)
3n-Doped v2	−3.67	−1.38	2.29
	(1.84)	(0.14)	(−1.70)

Tables 2 and 3. The computed HOMO–LUMO gap of pristine phenalene is 4.0 eV. With the original HOMO at −5.5 eV, n-doping leads to the occupation of more states and the HOMO's increase to −3.3 and −3.7 eV for single and triple concentrations, respectively. p-Doping of phenalene leads to a decrease of the LUMO level through the emptying of states to −3.9 and −4.2 eV with one and three dopants, respectively.

Deprotonated phenalene has in our model calculations a gap of 1.9 eV, which is contracted due to the removed hydrogen atom. The effect of p- and n-doping is smaller compared to the one in the phenalene molecule. In particular, the LUMO shifts by only 1.2 eV to lower energies whereas the HOMO increases now by only 1.0 eV. These shifts are observed with three dopant atoms. With a single dopant, the effect is even weaker.

The mechanism and the effects of doping on the electronic structure in phenalene and deprotonated phenalene are therefore the same as seen in coronene and are general.

Table 3 Energy levels of deprotonated phenalene's HOMO and LUMO and its doped versions. Values in brackets give the change relative to the pristine case

	HOMO (eV)	LUMO (eV)	Gap (eV)
p-Doped v2	−5.65	−3.96	1.69
	(−0.98)	(−1.17)	(−0.19)
p-Doped v1	−5.47	−3.50	1.97
	(−0.79)	(−0.71)	(0.09)
Pristine	−4.68	−2.80	1.88
n-Doped v1	−4.09	−1.88	2.21
	(0.59)	(0.92)	(0.33)
n-Doped v2	−3.70	−1.83	1.87
	(0.98)	(0.97)	(−0.09)

Carboxyl group molecules. Table 4 compares the energies of the HOMO, LUMO and the HOMO–LUMO gap for the version one (v1) and version two (v2) doping of the Na_2TP salt (Fig. 2). As mentioned above, v1 has a pyridine-like ring structure, whereas v2

13200 | *Phys. Chem. Chem. Phys.,* 2017, **19**, 13195–13209

This journal is © the Owner Societies 2017

Table 4 HOMO and LUMO eigenvalues of disodium terephthalate and its doped versions. Values in brackets give the change relative to the pristine system

	HOMO (eV)	LUMO (eV)	Gap (eV)
Pristine	−7.73	−2.59	5.14
p-Doped v1	−6.97	−2.61	4.36
	(0.76)	(−0.01)	(−0.78)
n-Doped v1	−7.73	−2.86	4.87
	(0.00)	(−0.27)	(−0.27)
p-Doped v2	−5.63	−3.48	2.16
	(2.10)	(−0.88)	(−2.98)
n-Doped v2	−3.12	−1.58	1.54
	(4.62)	(1.02)	(−3.60)

contains the dopant at a quasi-fused-ring position. In v1, the overall chemical structure is missing an H atom. Thus, v1 is not strictly substitutional doping. This becomes obvious if the total amount of electrons is analysed. In the case of n-v1, *i.e.* an n-doped v1 TP, the loss of the H atom compensates the occupation of an otherwise newly occupied state. The equivalent of p-doping, *i.e.* p-v1, has two fewer occupied states than the pristine salt.

The resulting HOMO and LUMO energy levels as well as the HOMO–LUMO (HL) gaps are compiled in Table 4. The molecular structures can be seen in Fig. 2. The HL-gap has a value of 5.1 eV for TP, with the HOMO at −7.7 and the LUMO at −2.6 eV.

The DOS of the pristine and the doped Na_2TP are shown in Fig. 6. Together with the frontier orbitals of Na_2TP and its doped versions shown in Fig. 7, insights into the effects of substitutional doping on the molecular, orbital and electronic structures, and in particular on the role of the redox-active carboxyl groups, can be gained.

For v1, introducing a B atom through a substitutional reaction leads to an increase of the HOMO by 0.76 eV while the LUMO is barely affected, see Table 4. The situation is reversed if an N atom is hosted in the ring structure. Then the HOMO barely shifts while the LUMO is stabilized by −0.27 eV. It follows that the contraction of the HL gap is also less significant *vs.* doped GFs. The contractions are −0.77 and −0.26 eV for p-doped v1 (p-v1) and n-doped v1 (n-v1), respectively. This can also be seen in the valence band in Fig. 6. Besides the changes in the position of the HOMO and LUMO levels of these systems, additional modifications can be noticed in states below the HOMO and above the LUMO. Doping affects therefore the whole electronic structure. The orbitals shown in Fig. 7 illustrate this point. The nodal structure of the doped systems undergoes a variety of changes. In pristine and n-doped v2 Na_2TP, the HOMOs have a similar nodal structure. The p-doped v1 has no frontier orbitals in common with the pristine molecule. This is caused by large structural and electronic structure changes. On the other hand, the n-doped Na_2TP v1 has a sodium centred LUMO and LUMO+1 similar to the pristine molecule. p-Doped v2 has less structural changes than p-doped v1 and the unoccupied orbitals of doped Na_2TP v2 are similar to those of n-doped Na_2TP v2. Other orbitals of p-doped Na_2TP v2 than the ones shown here have similar nodal structures to orbitals in pristine Na_2TP but different ordering indicating a strong orbital reordering due to doping. This also applies to n-doped Na_2TP v2.
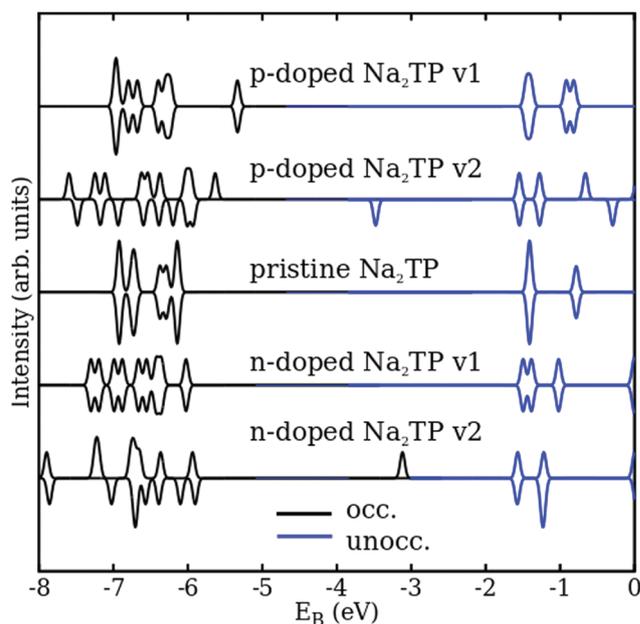

Fig. 6 DOS of pristine disodium terephthalate and its doped forms in the energy range between −8 and 0 eV. The occ. part of the DOS is given as black curve and the unocc. part is given as blue curve. The comparison between the doping approaches shows that only with type two (v2) doping a new occ. or unocc. state is created within the HOMO−LUMO gap of the pristine molecule.

The electronic and structural changes for doping of version one and two are therefore very different. While the substitutional doping in version 1 can also be used to change the electronic structure of materials to improve their performance as active battery components, it is not in line with the approach of substitutional doping we aim to achieve here. In contrast, it is the opposite of what would have been expected from this approach. This difference becomes more evident in comparison with v2.

With v2-type doping, all H atoms remain in the molecule. Thus, it exhibits much larger shifts as well as a larger contraction of the HL gap. The gap contractions are −3.0 and −3.6 eV for p-v2 and n-v2, respectively. These contractions are of similar order to the ones seen in the coronene case. Consequently, the HOMO and LUMO energies are more affected. The analysis of the HOMO and LUMO shifts is less straightforward because of the more involved electronic structure caused by hybridization effects. Nonetheless, an overall similarity to the coronene case can be identified. In particular, the p-v2 LUMO (−3.5 eV) is at a lower energy than that of n-v2 (−1.6 eV). The HOMO and LUMO follow the trends seen in the coronene case. For p-v2, the HOMO is at −5.6 eV and it is at −3.1 eV for n-v2. The HOMO in both cases, *i.e.* p- and n-doping, experiences the largest shift and in contrast to the coronene case, p-doping leads to an increased energy of the HOMO. Only the difference in the directions of LUMO shifts between p-v2 and n-v2 remains strong evidence for the doping effect.

Table 5 compiles the HOMO, LUMO energies and gap values for the disodium naphthalate (frTP) molecule and its doped versions, which are shown in Fig. 3. The pristine version has a
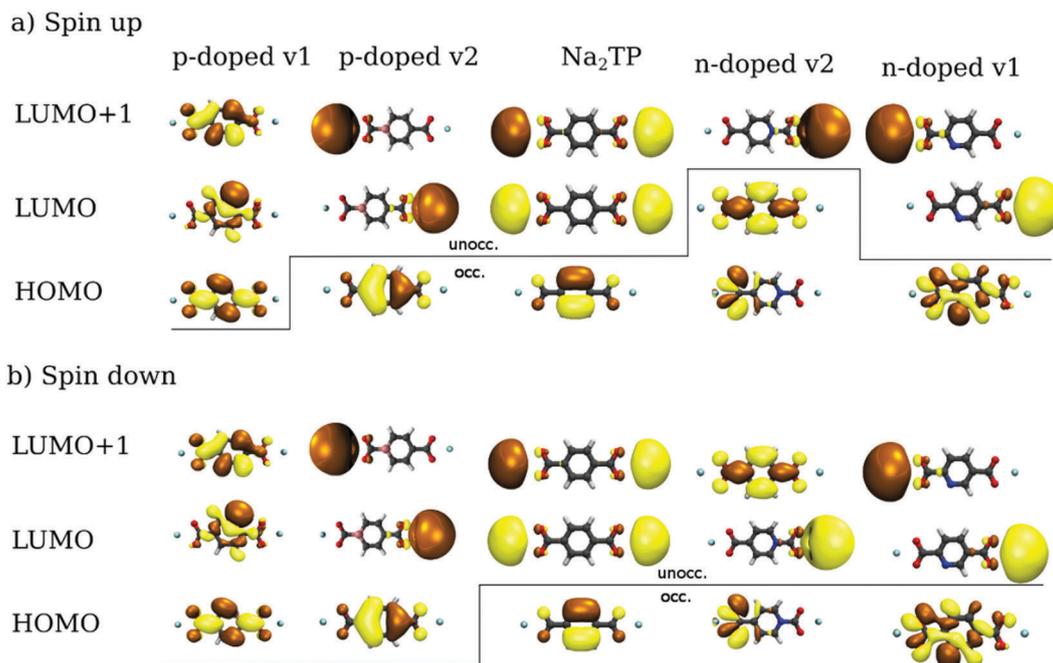
This journal is © the Owner Societies 2017

Phys. Chem. Chem. Phys., 2017, **19**, 13195–13209 | **13201**

Fig. 7 Spin up (a) and spin down (b) orbitals of the pristine disodium terephthalate and its doped versions. Occupied and unoccupied orbitals are separated with a solid black line. Different phases of the orbitals are shown as yellow and orange iso-density surfaces at values of 0.02 $e^{0.5}$ Å^{-3}. The labelling of the orbitals, *i.e.* HOMO, LUMO and LUMO+1 refers to those of the pristine disodium terephthalate molecule. Their counterparts in the p- and n-doped versions are drawn inline to the orbitals of the pristine molecule.

HL gap of 3.9 eV with its HOMO and LUMO at energies of −5.4 and −1.5 eV, respectively. Compared to the smaller Na$_2$TP salt, the energy levels are contracted which is a result of the larger size of the molecule.

Single p-doping at the site between two benzene rings, *i.e.* v1, shifts the HOMO by −0.2 eV and the LUMO by −2.2 eV down. Single n-doping affects the LUMO and HOMO in the opposite way. It lifts up the HOMO by 2.7 eV and stabilizes the LUMO by −0.57 eV. The doping-induced changes are weaker for frTP than in the case of the smaller Na$_2$TP salt, *e.g.* compared to v2 of TP.

In version two of frTP, the dopant is located at the quasi-fused ring position close to the carboxyl group. In version three, the dopant is at the position between the benzene rings and an additional one is at the same site as in v2. These two doping forms, *i.e.* v2 and v3, appear more promising in terms of larger energy shifts of frontier orbitals. p-Doping of v2 and v3 lowers the LUMO by −1.9 eV and −2.2 eV, respectively. This is about three times larger than the shift in n-v1. On the other hand, n-doping increases the HOMO by around 2–3 eV for all versions (v1, v2 and v3) and the changes in the LUMO positions are one order of magnitude smaller (0.1–0.6 eV).

The observed major shifts in v2 and v3 are comparable in magnitude and direction with those seen in the coronene case: p-doping shifts the LUMO down and n-doping shifts the HOMO up.

These results show also that the position of the dopant is a critical design factor in the design of organic electrode materials. Interestingly, the proximity of the dopant to the carboxyl group, *i.e.* the quasi fused-ring position, has similar effects in Na$_2$TP and frTP in terms of the direction and magnitude of changes in frontier orbital energies.

Table 5 HOMO and LUMO eigenvalues of disodium naphthalate and its doped versions. Values in brackets give the change relative to the pristine system

	HOMO (eV)	LUMO (eV)	Gap (eV)
Pristine	−5.40	−1.46	3.95
p-Doped v1	−5.21	−3.67	1.54
	(−0.18)	(−2.21)	(−2.41)
p-Doped v2	−5.35	−3.39	1.97
	(0.05)	(−1.93)	(−1.98)
p-Doped v3	−5.33	−3.68	1.65
	(0.07)	(−2.22)	(−2.29)
n-Doped v1	−2.75	−2.03	0.72
	(2.66)	(−0.57)	(−3.23)
n-Doped v2	−3.16	−1.65	1.51
	(2.25)	(0.19)	(−2.44)
n-Doped v3	−3.18	−1.59	1.59
	(2.22)	(0.14)	(−2.36)

Effect of doping on the attachment strengths of alkali atoms

While HOMO and LUMO designs are key features for understanding the voltage curve in organic electrode materials, it is also important to consider other molecular orbitals to understand possibilities for capacity control when multiple charge carriers (*i.e.* Li/Na atoms) are attached to a molecule.[32] In the following, lithiation/sodiation with the attachment of single or multiple Li/Na atoms is studied.

Graphene flakes: coronene. The attachment of Na and Li cations onto coronene happens at the center of the GF (*i.e.* not

13202 | *Phys. Chem. Chem. Phys.*, 2017, **19**, 13195–13209

This journal is © the Owner Societies 2017

at the edges of the flake). The alkali atoms bind the strongest on the hcp sites of the GF. When several alkali atoms bind to the GF, bridge sites are also occupied. At low alkali atom concentrations, the consecutive attachment of atoms happens in an alternating order on both sides of the coronene and its doped forms. Details are given in the ESI.† While the coronene molecule is flat, the binding of alkali atoms causes minor structural distortions, also in the direction out of the molecular plane. These changes are comparable to the ones seen in the single and triple p-doped systems without attachment of alkali atoms. The structural changes in the n-doped molecules are larger to some extent but without breaking any bonds in coronene.

We studied the attachment of multiple Li/Na atoms. For each number of attached atoms n (eqn (1)), the configurations with the lowest (strongest) binding energy can be used to compute effective voltage curves for lithiation and sodiation (see eqn (2)) of coronene in its pristine as well as its single and triple p- and n-doped forms. These are shown in Fig. 8(a) and (b) respectively. In these curves, a negative voltage (dashed lines) implies a regime where Li/Na atoms prefer to cluster (what would lead to the so-called "plating"). In this regime, the material cannot perform as an active electrode material. Furthermore, the dotted lines indicate the voltage curves expected taking into account segregation. In this case, the consecutive attachment of an increasing number Li/Na atoms does not follow a monotonic tend in the interaction strength. As a result, different numbers of Li/Na atoms will attach to different molecules.[75]

The lithiation of coronene with one to four atoms happens at voltages between −1.3 (single attachment) and −1.2 V (quadruple attachment), indicated by circles in Fig. 8(a). The voltage generally decreases with higher concentration of Li atoms for positive voltages and tends to 0 for negative voltages. In the case of sodiation, the voltages are in the range between −1.1 and −0.7 V when one to four Na atoms are attached. Since the voltages are below 0, coronene is not a suitable material for organic electrodes operating through the direct attachment of lithium/sodium.

Single p-doping shifts the initial voltage to positive values. The attachment of the first Li/Na atom has the strongest binding energy. The newly created empty state strengthens this binding. Starting at a voltage of 1.4 V, multiple lithiation rapidly decreases the voltage to 0.3 V at double and to −0.2 V at triple lithiation. During sodiation, the voltages reduce from an initial value of 1.2 to 0.2 and −0.1 V at single, double and triple attachments, respectively. In general, the first attachment benefits most from p-doping and its electric structure changes. For further attachments of alkali atoms, the effect is weaker. Since the voltage is approximately between 0 and 2 V for lithiation/ sodiation, single p-doped coronene can be used as an organic anode material.

For the higher concentration of p dopants (triple doped – v2), the voltages increase also to 1.4 and 1.1 V for the attachment of a Li and a Na atom, respectively. Moreover, the voltages remain positive and larger than 1 V even at high concentrations of cations. However, the voltages rapidly drop with further attachment. For example, at an attachment of six Li or six Na atoms the voltage is about 0.5 V.
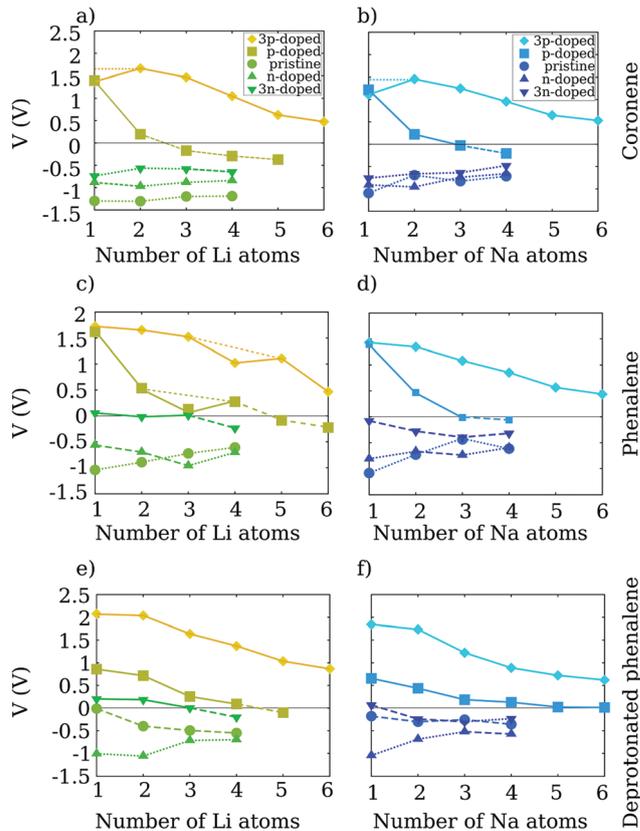

Fig. 8 Calculated voltages for lithiation (left panels) and sodiation (right panels) of coronene (a and b), phenalene (c and d) and deprotonated phenalene (e and f) in their pristine and doped forms. The voltages are shown with respect to Li/Li$^+$ (a, c and e) and Na/Na$^+$ (b, d and f). The voltages of the pristine systems are indicated here and elsewhere by circles, of the p-doped systems by squares and of the n-doped systems by triangles. Dotted lines indicate expected phase segregation and dashed lines indicate formation energies lower than the cohesive energy of the respective metal.

Interestingly, single and triple n-doping for the coronene molecule also increases the voltages for lithiation/sodiation. Comparing the strain contributions to the Li binding energy between pristine, p- and n-doped coronene reveals the reason. For the attachment of one Li atom, the strain energies in pristine and p-doped (v1 and v2) are *ca.* 0.1 eV while the strain energies are five times larger, *ca.* 0.5–0.6 eV, for the two n-doped coronene molecules (v1 and v2), see Table 6. The strain energies for the attachment of one Na atom are similar: 0.3 eV for the pristine, 0.1 for the p-doped (v1 and v2) and 0.4 to 0.5 eV for both n-doped versions, see Table 7. Therefore, the increased instability leading to larger strain energy is the reason for the increased voltage for the n-doped systems. In crystals, this contribution is unfavourable since it leads to thermodynamically unfavourable conditions, which occur, for example, during the insertion of Na atoms into silicon.[76] As can be seen in Fig. 8(a) for Li and in Fig. 8(b) for Na, n-doping cannot increase their binding strength enough to reach positive voltages, even though the initial voltages for both alkali atoms are raised to values of about −0.9 V for single and to *ca.* −0.8 V

Table 6 Strain energy (eV) for the attachment of one lithium atom onto pristine coronene, phenalene, deprotonated phenalene, disodium terephthalate and disodium naphthalate and their doped versions

	p-Doped			Pristine	n-Doped		
	v1	v2	v3		v1	v2	v3
Coronene	0.07	0.15	—	0.12	0.64	0.51	—
Phenalene	0.13	0.33	—	0.18	0.55	0.84	—
Deprotonated phenalene	0.04	0.64	—	0.08	0.05	0.17	—
Disodium terephthalate	—	0.30	—	1.02	—	0.06	—
Disodium naphthalate	0.0	0.18	0.16	0.17	0.92	1.62	1.29

for triple doping. The voltage curves for lithiation and sodiation are almost flat with respect to the degree of lithiation/sodiation. The overall electro-chemical lithiation/sodiation properties remain similar to those of coronene. While the increase in voltages, although still below 0 V, might be seen as a positive indication, this increase happens for reasons other than the electronic (and specifically band) structure changes due to doping. It is due to structural meta-stability introduced in the n-doped flakes. The single and triple n-doped coronene molecules show more structural changes during lithiation/sodiation. A comparable effect is well known from graphene, in which structural defects introduced *via* N atoms can improve the performance of graphene as an active battery material.[77]

Graphene flakes: phenalene ($C_{13}H_{10}$). The binding of an increasing number of alkali atoms happens with a preference for hcp locations. At low alkali atom concentrations, the consecutive attachment of atoms happens in an alternating order on both sides of the molecule. Overall, the adsorption mechanics appear to be very similar to the one seen with the coronene molecule. However, large structural changes due to the attachment of alkali atoms were observed for triple and single n-doped phenalene. Triple doping (p and n) causes more structural deformation than single doping. The p-doped structures were flat or almost flat during alkali attachment. The n-doped cases showed more structural instability.

Fig. 8(c) and (d) show the estimated potential curves of these phenalene systems for lithiation and sodiation, respectively. For the interaction of the pristine molecule with Li and Na cations, indicated by circles in the Fig. 8(c) and (d), the attachment of the first cation results in a potential of *ca.* −1 V. The lithiation and sodiation voltage curves of pristine phenalene are very similar to the ones of coronene. For both cations, the voltage curve begins at an initial value of around −1 V or slightly lower while the slope is relatively flat. The attachment of up to four cations monotonically reduces the voltage to *ca.* −0.6 V.

Table 7 Strain energy (eV) for the attachment of one sodium atom onto pristine coronene, phenalene, deprotonated phenalene, disodium terephthalate and disodium naphthalate and their doped versions

	p-Doped			Pristine	n-Doped		
	v1	v2	v3		v1	v2	v3
Coronene	0.07	0.10	—	0.31	0.56	0.43	—
Phenalene	0.1	0.34	—	0.00	0.85	0.65	—
Deprotonated phenalene	0.04	0.62	—	0.06	0.16	0.09	—
Disodium terephthalate	—	0.18	—	0.06	—	0.06	—
Disodium naphthalate	0.03	0.13	0.06	0.10	0.00	0.62	0.06

When single p-doped, the voltages are 1.6 V Li and 1.4 V for Li and Na attachment onto phenalene, respectively. The voltages reduce by about 1 V upon the attachment of a 2nd cation. For Na, the voltage close to 0 V is already reached after the 2nd Na attaches while for Li this occurs when more than three Li cations are attached.

In both cases, lithiation and sodiation, the here studied triple p-dopant concentration adds a potential of about 200 mV for the initial attachment of alkali atoms compared to the single p-doped case. The lithiation of triple p-doped phenalene provides a voltage between 1.7 and 1.5 V for the first three lithium atoms attached, Fig. 8(c). Thereafter, the binding weakens and the voltage reduces to *ca.* 1 V and it reaches 0.5 V at six Li atoms attached. For sodiation, the situation is similar but the shifts in the voltages caused by the additional dopants are smaller. After the attachment of two Na atoms, the voltage reduces to 1.0 V and it drops to *ca.* 0.5 V for six Na atoms, Fig. 8(d).

Similar to the coronene molecule, n-doping of phenalene does not seem to be a practical strategy to improve voltage. With a single dopant, the voltages remain between −0.8 and −0.6 V for Li and Na batteries. Triple doping increases the voltages to positive values for Li. However, the values remain close to 0 V. For sodiation, voltages close to 0 V were reached while they are still not positive. Single or triple n-doped molecules as well as the pristine phenalene therefore cannot be used as active electrode materials according to this model (*i.e.* without any help from environmental effects). Also for the phenalene molecule, the strain energies being larger than 0.6 eV for the first attachment of Li/Na are larger when the molecule is n-doped.

Graphene flakes: deprotonated phenalene ($C_{13}H_9$). The structural changes in deprotonated phenalene (DPH) follow the trends seen above. The pristine molecule keeps its planar structure during attachment of Li/Na. Interestingly, single p- and n-doped molecules also remain mostly planar. Only the triple doped versions deform slightly.

The theoretical voltage curves of pristine and doped deprotonated phenalene for the lithiation and sodiation are given in Fig. 8(e) and (f), respectively. The voltages for the pristine DPH are in the range between 0 and −0.5 V for Li and −0.2 and −0.4 V for Na. The voltages for $BC_{12}H_9$, *i.e.* single p-doped DPH, are between 1.0 V, for the attachment of one Li atom, and 0.1 eV for the attachment of up to four Li atoms. After two Li atoms are attached, the voltage profile drops significantly from 0.8 to 0.3 V. For the attachment of Na atoms, the voltage has an initial value of 0.7 V and reduces to 0.4 V for two Na atoms. The triple p-doped systems show a large shift to positive voltages for the interaction with Na and Li cations. With Li/Na cations, the voltage profile starts at 2.1/1.8 V. The voltage reduces to 0.9/0.6 V with an attachment of six atoms Li/Na which indicates a large capacity. Moreover, this shows that single and triple p-doping can make deprotonated phenalene a promising organic anode material.

For the single n-doped DPH, the initial lithiation/sodiation voltage starts at −1.0/−1.0 V and reduces to *ca.* −0.7/−0.6 V

13204 | *Phys. Chem. Chem. Phys.*, 2017, **19**, 13195–13209

This journal is © the Owner Societies 2017

when four/three Li/Na atoms are attached. With regard to application as an electrode material, n-doped DPH appears unlikely to be usable for Li and Na batteries that work by reduction. In contrast to the previous cases, single n-doping weakens the binding between the molecule and Li/Na atoms compared to the pristine DPH. For triple n-doping, the voltages, although increased, are not significantly different from 0 V, similar to the results for the phenalene molecule. However, this effect might be more associated to structural changes introduced by instabilities through triple doping.

As mentioned above, structural changes can explain the increase in voltage for n-doping better than changes in the band structure induced by doping. We observed that the structures of the single and triple n-doped phenalene molecules are more sensitive to the attachment of cations than their p-doped counterparts. The influence becomes more evident with increasing concentration of alkali atoms. For instance, $N_3C_{10}H_{10}$, *i.e.* triple n-doped phenalene, shows more deformation during lithium attachments because of the larger structural instability. In contrast, $B_3C_{10}H_{10}$ remains a flat molecule under the attachment of Li/Na atoms. This difference can already be seen during the first attachment for which the strain energies in n-doped phenalene are larger than those in p-doped phenalene, see Tables 6 and 7. This points out that n- and p-doping can serve different purposes in practice. Although in both cases the changes in the electronic structure are as expected with n- and p-doping (and are similar to those observed when doping solid semiconductors), the use of n- and p-doping implements two different design strategies: n-doping can lead to increased battery performance through structural changes (meta-stability which strengthens Li/Na binding energy),[17] whereas p-doping modifies the binding to the alkali atoms through creation of electronic vacancies, *e.g.* the band structure design.

The presented results for doped carbon flakes (coronene, phenalene, and deprotonated phenalene) are very similar, which points to their general nature. p-Doping can drastically increase the voltage for organic materials by means of electronic structure modifications. It also can increase theoretical capacities. In contrast, n-doping can make use of structural instabilities to modulate the voltage of an organic material.

In the following, we elaborate the effects due to doping in the case of molecules with redox active centres. As mentioned above, we choose the disodium terephthalate and the disodium naphthalate each having two carboxyl groups for this purpose.

Carboxyl group molecules: disodium terephthalate. The adsorption structures of Na_2TP and its doped versions (v2) having one to six sodium or lithium cations attached are very similar. The first few attachments happen close to the carboxylic groups and, in case of doping, in the vicinity of the doped site. At larger concentrations, the cations interact more with the aromatic ring of the molecule before clustering occurs. The lithiation on Na_2TP involves reduction of the Na^+ cation and the charge compensation of the additional electron on the TP-compound by an incoming Li atom. The respective Mulliken charges on the sodium atoms confirm that. In the pristine Na_2TP, there are 0.9 electrons removed on each of the sodium

atoms according to the Mulliken analysis. The attachment of a lithium atom reduces this to 0.5 electrons. The Li charge is +0.4. Interestingly, the change is smaller when a Na atom is attached. Then, the charge on the attached Na is +0.3. Therefore, Li donates more charge to Na_2TP. A similar process was suggested before for the Ag_2TP anode.[54]

The pristine Na_2TP molecule has a stable structure during the attachment of Li/Na atoms. Its p-doped version changes the dihedral angle between the carboxyl group and the benzene ring when Li/Na atoms bind to it. Interestingly, this results in larger strain energies for p-doping than for n-doping, see Tables 6 and 7, since the dihedral angle remains that of the pristine molecule in the latter case. The structural changes in n-doped Na_2TP are very different. While it remains flat for the first attachments (1–2 atoms), the molecule bends for larger amounts of alkali atoms binding to it.

Pristine (molecular) Na_2TP lacks a strong interaction with Li/Na atoms to be a working anode material. The theoretical voltages for lithiation and sodiation are shown in Fig. 9(a) and (b), respectively. For one to four atoms attached, the voltages are between −0.4 and −0.2 V for attachment of Na atoms and between −0.6 and −0.2 V for lithium atoms. However, effects due to crystal structure, porosity and disorder can have an substantial effect on the performance of batteries.[78–80] In particular, recent theoretical studies showed that covalent and van der Waals crystals can lead to an additional voltage by 0.2 to 0.7 eV in the interaction strength between Li/Na and an organic molecule.[28,32,33,51,75] Thus, molecules with a small negative voltage can perhaps become useable electrode materials in their crystal phase.

p-Doping leads to a substantially stronger binding to Li (Na) so that p-doped Na_2TP would act as an anode material, as shown in Fig. 9(a) and (b), with an initial voltage of 1.9 V (lithiation) and 1.8 V (sodiation). The lithiation (sodiation) voltage decreases to 0.8 (0.8), 0.6 (0.5) and 0.2 (0.3) V at double, triple and quadruple attachment, respectively. This is of course expected as the empty state created by the doping will have the strongest effect for the first attached Li/Na, whose valence electron fills it. For n-doping, the voltage profile remains very similar to the one of Na_2TP with values between −0.1 and −0.2 V for lithiation and −0.4 and −0.2 V for sodiation for the attachment of one to four atoms.

Carboxyl group molecules: disodium naphthalate. Similar to the Na_2TP salt, the initial attachment of Li/Na atoms onto disodium naphthalate takes place near the carboxylic groups. Interestingly, it happens close to the dopant for p-doping while for n-doping it is on the carboxylic group that is not bonded to the dopant.

The pristine frTP molecule remains flat when lithiated/ sodiated. In its p-doped versions, the dihedral angles between carboxyl groups and benzene rings change through the attachment of Li/Na atoms (similar to the p-doped Na_2TP). When n-doped, the attachment of Li/Na atoms can cause larger changes in the structure. Bending of the molecule was observed for Na attachments onto n-doped v1 and for Li attachments onto n-doped v3.

The voltage profiles of frTP are shown in Fig. 9(c) for lithiation and in Fig. 9(d) for sodiation. Like the Na_2TP salt, the frTP has a negative voltage of *ca.* −0.4 in both Li and Na

This journal is © the Owner Societies 2017

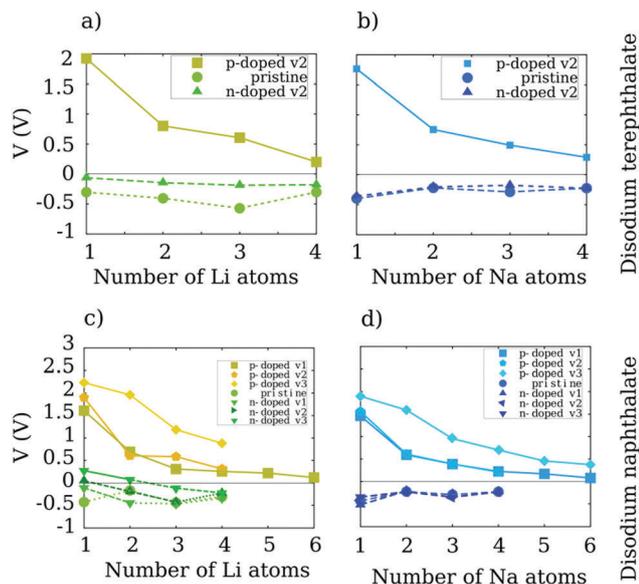*Phys. Chem. Chem. Phys.,* 2017, **19**, 13195–13209 | **13205**

Fig. 9 Calculated voltages for lithiation (left panels) and sodiation (right panels) of disodium terephthalate (a and b) and disodium naphthalate (c and d) in their pristine and doped forms vs. Li/Li$^+$ (a and c) and vs. Na/Na$^+$ (b and d). Dotted lines indicate phase segregation and dashed lines indicate formation energies lower than the cohesive energy of the respective metal.

Table 8 Averaged, minimal and maximal change in voltage (ΔV) of all systems in this study during lithiation/sodiation caused by p–doping relative to the pristine molecules for one (1B), two (2B) and three (3B) dopants. All values given in V

p-Doped		1B	2B	3B
Li	Average ΔV	2.11	2.62	2.53
	Min ΔV	0.87	—	2.14
	Max ΔV	2.69	—	2.77
Na	Average ΔV	1.84	2.33	2.35
	Min ΔV	0.83	—	2.02
	Max ΔV	2.34	—	2.52

Table 9 Averaged, minimal and maximal change in voltage (ΔV) of all systems in this study during lithiation/sodiation caused by n–doping relative to the pristine molecules for one (1N), two (2N) and three (3N) dopants. All values given in V

n-Doped		1N	2N	3N
Li	Average ΔV	0.43	1.51	0.62
	Min ΔV	−1.00	—	0.21
	Max ΔV	1.29	—	1.10
Na	Average ΔV	−0.04	0.04	0.57
	Min ΔV	−0.87	—	0.06
	Max ΔV	0.50	—	1.01

batteries. p-Doping increases the voltage for frTP v1 to 1.7 (1.5) V for one Li (Na) attachment. However, the voltage drops thereafter significantly to a value of 0.7 (0.6) V for double attachment, see Fig. 9(c) and (d). When the dopant is between the benzene rings of frTP, i.e. v2, the voltages are similar to the voltages in the p-doped frTP v1. Specifically, the initial voltage is about 1.9 (1.6) V and drops with further attachment of Li (Na) atoms to values of 0.6–0.3 (0.6–0.2) V. Only increasing the dopant concentration in the molecule has a substantial effect on the voltage profile. This is achieved in v3 where the quasi- and the fused-ring positions, i.e. v1 and v2, are doped simultaneously. Then, the initial voltage increases to 2.2 (1.9) V for lithiation (sodiation). For p-doped frTP v3, attachment of further Li/Na atoms results in consecutive voltages of 2.0 (1.6), 1.2 (1.0) and 0.9 (0.7) V.

Comparing p-doped v1, v2 and, v3 frTP when lithiated/sodiated, the voltage profiles appear rather similar at voltages of ca. 2.0 V. However, the voltages of v1 and v2 drop below 1.0 V already for the second attached atom while the voltage remains larger 1.5 V for v3 when up to two alkali atoms attach. This is a result of the higher p-dopant concentration. Therefore, the expected capacity per molecule is larger for v3 than for v1/v2. Interestingly, n-doping is most beneficial for the attachment of Na atoms if the dopant is in vicinity of the carboxyl group, i.e. v2. This can be understood from the large strain energy of 0.6 eV in this configuration, see Table 7. This effect also causes in the case of lithiation for v2 and v3 to have large strain energies (1.6 and 1.3 eV), see Table 6. Sodiation for the other two n-doped versions (v1 and v3) leads to voltages of about −0.4 V for the initial attachment and the voltage increases to slightly larger values (but still below 0 V) for multiple attachments.

Tables 8 and 9 summarize the effect of p- and n-doping, respectively, on the voltage for all molecules investigated in this study at the first attachment of one Li/Na atom. The averaged, minimal and maximal voltage changes are obtained for all doped systems relative to their pristine systems. The summarized results show that p-doping can increase the voltage by at least 0.9 (0.8) V for lithiation (sodiation). Moreover, the increase in voltage is on average 1 to 2 V larger for p-doping than for n-doping. Among the studied systems, the change can reach 2.8 (2.5) V. An increase in voltage can be observed with increasing number of dopants. However, n-doping does not necessarily result in an increased voltage. Nonetheless, the average gain in voltage is 0.4, 1.5 and 0.6 V for single, double and triple n-doping during lithiation. For sodiation, the effect is weaker and changes in the voltage are smaller. Both p- and n-doping lead to a contraction of the HOMO–LUMO gap which may be beneficial for conductance and therefore rate performance.

Discussion

At this point, we have presented five systems with and without redox active groups. In both cases, the observed effects of p- and n-doping are of similar nature. From an electronic structure perspective, p-doping creates vacancies which lead to a stabilization of the LUMO. The resulting shift in orbital energy leads to an increased interaction strength between Li/Na atoms and the molecule, since the transferred electron of the reduction occupies the stabilized LUMO. With increasing number of p-dopants, the LUMO stabilised more. The larger the shift towards lower energies is, the larger is the potential increase in voltage for active battery materials. This was

specifically observed comparing single with double or triple p-doped systems, in which multiple doping achieves larger voltages and stabilization of the new LUMO, see Table 8. This holds for a molecule without redox active groups, for example coronene, phenalene and deprotonated phenalene, as well as with redox-active groups seen in disodium terephthalate and disodium naphthalate. For n-doping in most cases discussed here, electronic effects cause a small stabilization of the LUMO while creating a newly occupied state. However, the shifts seen are one order of magnitude smaller than in the case of p-doping. Often n-doping also introduces instability in the molecular structure. The resulting strain energy in n-doped systems can reach more than 1.6 eV, see Table 6. The strain energies seen in p-doped systems are in general smaller than those seen in n-doped systems. Additional environmental effects may invert this as seen in the case of deprotonated phenalene. The strain energy can contribute to the voltage in addition to the purely electronic effects. Interestingly, these effects only apply in the case of substitutional doping described above and not in the case of a substitutional reaction if other structural changes occur simultaneously with it.

Fig. 10 and 11 summarize the LUMO energy shifts compared to the change in voltage at an attachment of one Li and Na atom, respectively. The pristine molecules were taken as reference to obtain the energy shifts of the LUMOs and the changes in the voltages. In general, Li and Na attachment have very similar features in these plots. p-doped systems, indicated by empty markers in Fig. 10 and 11, have LUMO shifts between -0.5 and -3 eV while n-doped systems indicated by filled markers in Fig. 10 and 11, have shifts of *ca.* -1 to 1 eV. The voltage changes are 1.5 to -1.5 V for n-doping and 0.5 to 2.5 V for p-doping. Thus, the data points for the two doping approaches arrange in different parts of these plots. The largest voltage increase was achieved by p-doping whereas n-doping can also result in a
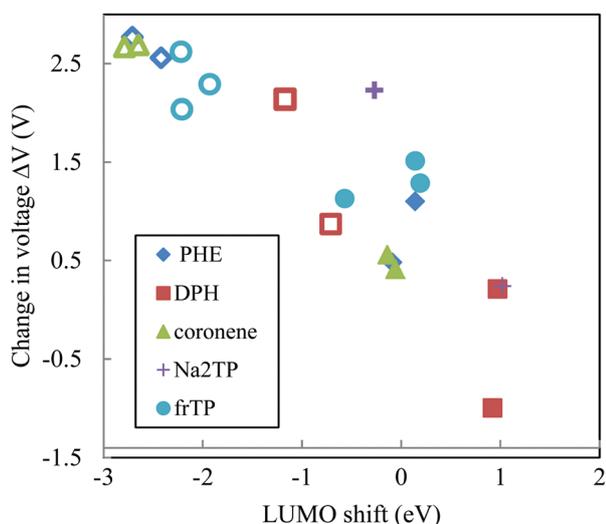

Fig. 11 LUMO shifts (eV) *vs.* change in voltages (ΔV) due to doping for the attachment of one Na atom onto coronene (green), phenalene (blue), deprotonated phenalene (red), disodium terephthalate (purple) and disodium naphthalate (light blue). The empty (filled) markers show data for p-doping (n-doping).
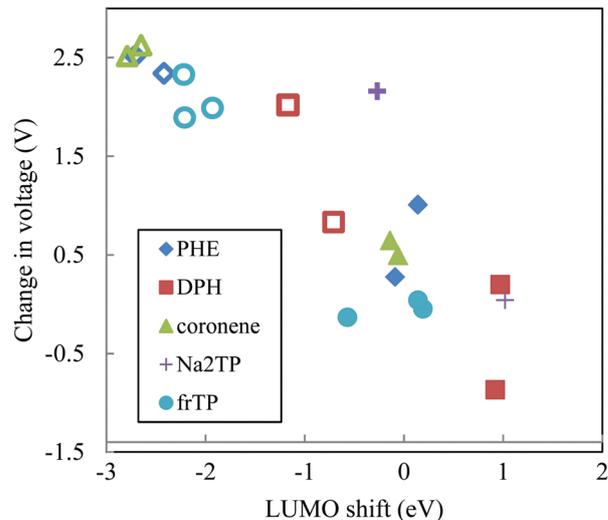
decreased voltage. Interestingly, the doped coronene and phenalene show a strong correlation between LUMO energy shifts and changes in voltage whereas the voltage-LUMO data points in deprotonated phenalene and the disodium naphthalate salt deviate more from a direct correlation. The larger spread could be caused by the larger strain energies in these systems. This points further to a complex interplay between contributions from strain and electronic structure to the binding energy/voltage in these systems.

From a purely experimental perspective, it is not easy to determine the mechanistic reasons for an increased or decreased performance of active organic electrode materials. Doping adds complexity to this problem which can be resolved with the help of theory. The presented results for the p- and n-doped systems show strong indications from an electronic structure perspective that p-doping is a better approach to increase the voltage by means of modulation of electronic structure. This was elaborated on materials for organic electrodes working by reduction. On the other hand, n-doping can also be used to improve battery performance, but in this case structural meta-stability is an additional factor that must be considered.

Conclusions

In this study, five prototypical organic systems were investigated by first principle methods for their performance as electrode materials in organic lithium and sodium batteries and their potential improvements gained from substitutional p- and n-doping. Substitutional doping can be applied to molecules with and without redox active centers and the achievable performance improvements are on the same order of magnitude for both cases. It is therefore a general ansatz that can be transferred to other molecular systems, and in particular, to molecules with other redox active groups.

Fig. 10 LUMO shifts (eV) *vs.* change in voltages (ΔV) due to doping for the attachment of one Li atom onto coronene (green), phenalene (blue), deprotonated phenalene (red), disodium terephthalate (purple) and disodium naphthalate (light blue). The empty (filled) markers show data for p-doping (n-doping).

We found that p-doping increases the voltage by *ca.* 2 V for the first attachment of Li/Na by electronic structure means, *i.e.* the newly created vacancy state. This applies to molecules with and without redox active groups. When a molecule is p-doped, the first Li/Na attachment experiences the largest change in binding energy between Li/Na atom and molecule. The voltage generally decreases with the attachment of further Li/Na atoms, but this decrease in voltage is reduced when the molecule contains more p-dopants. Thus, the capacity can be improved by increasing the amount of p-dopants. n-Doping can also improve voltages, but structural effects must be understood for this approach since structural instability is introduced leading to a large strain contributions to the binding energy. With the doping approach and in particular p-doping, non-working organic electrodes can become working anode materials. It also seems possible to modify existing anode materials to make them work as high voltage cathodes. Environmental conditions, such as the pH value or crystalline environment, can have a substantial effect on the mechanism and magnitude of the voltage improvements gained from p-doping.

Overall, electronic and structural contributions add up to the total binding strength/voltage. In general, p-doping strengthens the binding mainly by electronic and n-doping by structural effects even though this depends in detail on the particular system. A stabilising structure, like fused aromatic rings, is beneficial to distinguish the two effects.

Acknowledgements

References

1 C. F. Holmes, *ECS Trans.*, 2007, **6**(5), 1–7.

2 L. Wang, M. Zhao, J. Qiu, P. Gao, J. Xue and J. Li, *Energy Technol.*, 2017, **5**, 637.

3 J. G. Kim, B. Son, S. Mukherjee, N. Schuppert, A. Bates, O. Kwon, M. J. Choi, H. Y. Chung and S. Park, *J. Power Sources*, 2015, **282**, 299–322.

4 N. Alias and A. A. Mohamad, *J. Power Sources*, 2015, **274**, 237–251.

5 N. Nitta, F. Wu, J. T. Lee and G. Yushin, *Mater. Today*, 2014, **18**(5), 252–264.

6 Y. Wang, B. Liu, Q. Li, S. Cartmell, S. Ferrara, Z. D. Deng and J. Xiao, *J. Power Sources*, 2015, **286**, 330–345.

7 B. Diouf and R. Pode, *Renewable Energy*, 2015, **76**, 375–380.

8 M. Miroshnikov, K. P. Divya, G. Babu, A. Meiyazhagan, L. M. R. Arava, P. M. Ajayan and G. John, *J. Mater. Chem. A*, 2016, **4**(32), 12370–12386.

9 Y. Liang, Z. Tao and J. Chen, *Adv. Energy Mater.*, 2012, **2**(7), 742–769.

10 A. Barre, B. Deguilhem, S. Grolleau, M. Gerard, F. Suard and D. Riu, *J. Power Sources*, 2013, **241**, 680–689.

11 L. Lu, X. Han, J. Li, J. Hua and M. Ouyang, *J. Power Sources*, 2013, **226**, 272–288.

12 L. Wang, F. Zhou, Y. S. Meng and G. Ceder, *Phys. Rev. B: Condens. Matter Mater. Phys.*, 2007, **76**(16), 165435.

13 X. Yang, Z. Liu, X. Chen, W. Wang, X. Chen, Z. Yuan, H. Zhou, R. Zeng and Y. Luo, *J. Electroanal. Chem.*, 2016, **782**, 202–206.

14 A. M. Stephan and K. S. Nahm, *Polymer*, 2006, **47**(16), 5952–5964.

15 X. Zeng, J. Li and B. Shen, *J. Hazard. Mater.*, 2015, **295**, 112–118.

16 X. Zeng, J. Li and N. Singh, *Crit. Rev. Environ. Sci. Technol.*, 2014, **44**(10), 1129–1165.

17 F. Legrain, J. Sottmann, K. Kotsis, S. Gorantla, S. Sartori and S. Manzhos, *J. Phys. Chem. C*, 2015, **119**(24), 13496–13501.

18 P. Hartmann, C. L. Bender, M. Vracar, A. K. Dürr, A. Garsuch, J. Janek and P. Adelhelm, *Nat. Mater.*, 2012, **12**(3), 228–232.

19 S. Kang, Y. Mo, S. P. Ong and G. Ceder, *Nano Lett.*, 2014, **14**(2), 1016–1020.

20 Y. Chen, W. Luo, M. Carter, L. Zhou, J. Dai, K. Fu, S. Lacey, T. Li, J. Wan, X. Han, Y. Bao and L. Hu, *Nano Energy*, 2015, **18**, 205–211.

21 D. I. Williams, J. J. Byrne and J. S. Driscoll, *J. Electrochem. Soc.*, 1969, **116**(1), 2–4.

22 Q. Zhao, J. Wang, Y. Lu, Y. Li, G. Liang and J. Chen, *Angew. Chem.*, 2016, **128**(40), 12716–12720.

23 J.-K. Kim, J. Scheers, J.-H. Ahn, P. Johansson, A. Matic and P. Jacobsson, *J. Mater. Chem. A*, 2013, **1**(7), 2426–2430.

24 Y. Chen and S. Manzhos, *J. Power Sources*, 2016, **336**, 126–131.

25 A. J. Heeger, *J. Phys. Chem. B*, 2001, **105**(36), 8475–8491.

26 S. Muench, A. Wild, C. Friebe, B. Häupler, T. Janoschka and U. S. Schubert, *Chem. Rev.*, 2016, **116**(16), 9438–9484.

27 E. Geniès, P. Hany and C. Santier, *Synth. Met.*, 1989, **28**(1–2), 647–654.

28 M. A. Sk and S. Manzhos, *J. Power Sources*, 2016, **324**, 572–581.

29 K. Nakahara, S. Iwasa, M. Satoh, Y. Morioka, J. Iriyama, M. Suguro and E. Hasegawa, *Chem. Phys. Lett.*, 2002, **359**, 351–354.

30 J. Y. Zhang, L. B. Kong, L. Z. Zhan, J. Tang, H. Zhan, Y. H. Zhou and C. M. Zhan, *J. Power Sources*, 2007, **168**(1), 278–281.

31 R. D. Rauh, K. M. Abraham, G. F. Pearson, J. K. Surprenant and S. B. Brummer, *J. Electrochem. Soc.*, 1979, **126**(4), 523–527.

32 Y. Chen and S. Manzhos, *Phys. Chem. Chem. Phys.*, 2016, **18**(3), 1470–1477.

33 Y. Chen and S. Manzhos, *Mater. Chem. Phys.*, 2015, **156**, 180–187.

34 A. Guerfi, J. Trottier, C. Gagnon, F. Barray and K. Zaghib, *J. Power Sources*, 2016, **335**, 131–137.

35 H. Sano, H. Senoh, M. Yao, H. Sakaebe and T. Kiyobayashi, *Chem. Lett.*, 2012, **41**(12), 1594–1596.

36 F. Xu, H. Wang, J. Lin, X. Luo, S.-A. Cao and H. Yang, *J. Mater. Chem. A*, 2016, **4**(29), 11491–11497.

37 W. Humphrey, A. Dalke and K. Schulten, *J. Mol. Graphics*, 1996, **14**, 33–38.

38 V. Palomares, P. Serras, I. Villaluenga, K. B. Hueso, J. Carretero-Gonzalez and T. Rojo, *Energy Environ. Sci.*, 2012, **5**(3), 5884–5901.

39 I. A. Rodriguez-Perez, Z. Jian, P. K. Waldenmaier, J. W. Palmisano, R. S. Chandrabose, X. Wang, M. M. Lerner, R. G. Carter and X. Ji, *ACS Energy Lett.*, 2016, **1**(4), 719–723.

13208 | *Phys. Chem. Chem. Phys.*, 2017, **19**, 13195–13209

This journal is © the Owner Societies 2017

40 M. L. Aubrey and J. R. Long, *J. Am. Chem. Soc.*, 2015, **137**(42), 13594–13602.

41 Q. Zhao, Y. Lu and J. Chen, *Adv. Energy Mater.*, 2016, 1601792.

42 Q. Deng, C. Fan, L. Wang, B. Cao, Y. Jin, C.-M. Che and J. Li, *Electrochim. Acta*, 2016, **20**, 1086–1093.

43 L. M. Zhu, A. W. Lei, Y. L. Cao, X. P. Ai and H. X. Yang, *Chem. Commun.*, 2013, **49**(6), 567–569.

44 M. J. Momeni, E. Targholi and M. Mousavi-Khoshdel, *Comput. Mater. Sci.*, 2016, **124**, 166–172.

45 M. Molaei, S. M. Mousavi-Khoshdel and E. Targholi, *Curr. Appl. Phys.*, 2017, **17**(2), 272–278.

46 R. B. Araujo, A. Banerjee, P. Panigrahi, L. Yang, M. Stromme, M. Sjodin, C. M. Araujo and R. Ahuja, *J. Mater. Chem. A*, 2017, **5**, 4430–4454.

47 Y. Hanyu and I. Honma, *Sci. Rep.*, 2012, **2**, 453.

48 C.-P. Yang, Y.-X. Yin, H. Ye, K.-C. Jiang, J. Zhang and Y.-G. Guo, *ACS Appl. Mater. Interfaces*, 2014, **6**(11), 8789–8795.

49 R. Cao, J.-S. Lee, M. Liu and J. Cho, *Adv. Energy Mater.*, 2012, **2**(7), 816–829.

50 F. Legrain and S. Manzhos, *J. Power Sources*, 2015, **274**, 65–70.

51 M. A. Sk and S. Manzhos, *MRS Adv.*, 2016, **1**(53), 3579–3584.

52 Y. Park, D.-S. Shin, S. H. Woo, N. S. Choi, K. H. Shin, S. M. Oh, K. T. Lee and S. Y. Hong, *Adv. Mater.*, 2012, **24**(26), 3562–3567.

53 L. Zhao, J. Zhao, Y.-S. Hu, H. Li, Z. Zhou, M. Armand and L. Chen, *Adv. Energy Mater.*, 2012, **2**(8), 962–965.

54 J. Xue, C. Fan, Q. Deng, M. Zhao, L. Wang, A. Zhou and J. Li, *Electrochim. Acta*, 2016, **219**, 418–424.

55 M. Nisula and M. Karppinen, *Nano Lett.*, 2016, **16**(2), 1276–1281.

56 T. Yasuda and N. Ogihara, *Chem. Commun.*, 2014, **50**(78), 11565–11567.

57 N. Ogihara, T. Yasuda, Y. Kishida, T. Ohsuna, K. Miyamoto and N. Ohba, *Angew. Chem., Int. Ed.*, 2014, **53**(43), 11467–11472.

58 J. Frisch, G. W. Trucks, H. B. Schlegel, G. E. Scuseria, M. A. Robb, J. R. Cheeseman, G. Scalmani, V. Barone, B. Mennucci, G. A. Petersson, H. Nakatsuji, M. Caricato, X. Li, H. P. Hratchian, A. F. Izmaylov, J. Bloino, G. Zheng, J. L. Sonnenberg, M. Hada, M. Ehara, K. Toyota, R. Fukuda, J. Hasegawa, M. Ishida, T. Nakajima, Y. Honda, O. Kitao, H. Nakai, T. Vreven, J. J. A. Montgomery, J. E. Peralta, F. Ogliaro, M. Bearpark, J. J. Heyd, E. Brothers, K. N. Kudin, V. N. Staroverov, R. Kobayashi, J. Normand, K. Raghavachari, A. Rendell, J. C. Burant, S. S. Iyengar, J. Tomasi, M. Cossi, N. Rega, J. M. Millam, M. Klene, J. E. Knox, J. B. Cross, V. Bakken, C. Adamo, J. Jaramillo, R. Gomperts, R. E. Stratmann, O. Yazyev, A. J. Austin, R. Cammi, C. Pomelli, J. W. Ochterski, R. L. Martin, K. Morokuma, V. G. Zakrzewski, G. A. Voth, P. Salvador, J. J. Dannenberg, S. Dapprich, A. D. Daniels, Ö. Farkas, J. B. Foresman, J. V. Ortiz, J. Cioslowski and D. J. Fox, *Gaussian 09 Revision E.01*, 2016.

59 A. D. Becke, *Phys. Rev. A: At., Mol., Opt. Phys.*, 1988, **38**, 3098–3100.

60 S. H. Vosko, L. Wilk and M. Nusair, *Can. J. Phys.*, 1980, **58**(8), 1200–1211.

61 C. Lee, W. Yang and R. G. Parr, *Phys. Rev. B: Condens. Matter Mater. Phys.*, 1988, **37**, 785–789.

62 G. A. Petersson and M. A. Al-Laham, *J. Chem. Phys.*, 1991, **94**(9), 6081–6090.

63 G. A. Petersson, A. Bennett, T. G. Tensfeldt, M. A. Al-Laham, W. A. Shirley and J. Mantzaris, *J. Chem. Phys.*, 1988, **89**(4), 2193–2218.

64 E. Kaxiras, *Atomic and Electronic Structure of Solids*, Cambridge University Press, 2003.

65 C. Kittel, *Introduction to Solid State Physics*, Wiley, 2005.

66 A. Urban, D.-H. Seo and G. Ceder, *Npj Computational Materials*, 2016, **2**, 16002.

67 M. K. Aydinol, A. F. Kohan, G. Ceder, K. Cho and J. Joannopoulos, *Phys. Rev. B: Condens. Matter Mater. Phys.*, 1997, **56**, 1354–1365.

68 M. Armand, S. Grugeon, H. Vezin, S. Laruelle, P. Ribiere, P. Poizot and J.-M. Tarascon, *Nat. Mater.*, 2009, **8**(2), 120–125.

69 P. Tavhare, A. Deshmukh and A. Chaudhari, *Phys. Chem. Chem. Phys.*, 2017, **19**(1), 681–694.

70 K. S. Novoselov, A. K. Geim, S. V. Morozov, D. Jiang, Y. Zhang, S. V. Dubonos, I. V. Grigorieva and A. A. Firsov, *Science*, 2004, **306**(5696), 666–669.

71 Y. Shao, S. Zhang, M. H. Engelhard, G. Li, G. Shao, Y. Wang, J. Liu, I. A. Aksay and Y. Lin, *J. Mater. Chem.*, 2010, **20**(35), 7491.

72 L. S. Panchakarla, K. S. Subrahmanyam, S. K. Saha, A. Govindaraj, H. R. Krishnamurthy, U. V. Waghmare and C. N. R. Rao, *Adv. Mater.*, 2009, **21**(46), 4726–4730.

73 T. Lin, F. Huang, J. Liang and Y. Wang, *Energy Environ. Sci.*, 2011, **4**(3), 862–865.

74 H. Wang, T. Maiyalagan and X. Wang, *ACS Catal.*, 2012, **2**(5), 781–794.

75 Y. Chen and S. Manzhos, *Phys. Chem. Chem. Phys.*, 2016, **18**(13), 8874–8880.

76 F. Legrain, O. I. Malyi and S. Manzhos, *Comput. Mater. Sci.*, 2014, **94**, 214–217.

77 A. L. M. Reddy, A. Srivastava, S. R. Gowda, H. Gullapalli, M. Dubey and P. M. Ajayan, *ACS Nano*, 2010, **4**(11), 6337–6342.

78 A. D. Roberts, X. Li and H. Zhang, *Chem. Soc. Rev.*, 2014, **43**(13), 4341.

79 W.-b. Zhang, Z.-x. Zhang, J.-h. Yang, T. Huang, N. Zhang, X.-t. Zheng, Y. Wang and Z.-w. Zhou, *Carbon*, 2015, **90**, 242–254.

80 N. Mahmood, T. Tang and Y. Hou, *Adv. Energy Mater.*, 2016, **6**(17), 1600374.